

## NON-LINEAR DYNAMIC ANALYSIS OF AN AXIALY MOVING VISCOELASTIC BEAM

KRZYSZTOF MARYNOWSKI

*Department of Machines Dynamics, Technical University of Łódź  
email: kmarynow@ck-sg.p.lodz.pl*

Stability and oscillation characteristics of an axially moving beam have been investigated. Two different models of the beam material, i.e., Kelvin-Voigt and Maxwell have been considered. The numerical solutions of full nonlinear and linearized equations have been compared. The effects of axially travelling speed and the internal damping on dynamical stability of the axially moving beam have been studied in details. Numerical studies of the Kelvin-Voigt and Maxwell models show that both models give similar results only for small values of the internal damping (dimensionless internal damping coefficient smaller than  $5 \cdot 10^{-6}$ ). For materials with larger damping coefficient the considered models give different results.

*Key words:* moving beam, internal damping, dynamic stability

### Notation

$A$	–	cross section area of the beam
$b$	–	width of the beam
$c$	–	axial transport speed
$c_f$	–	wave velocity
$d$	–	thickness of the beam
$E$	–	Young's modulus of the beam material
$J$	–	cross section moment of inertia
$k_1, k_2, k_3$	–	dimensionless coefficients
$l$	–	length of the beam
$M$	–	bending moment

$N$	–	axial stress
$P$	–	tension force
$r_1, r_2, r_3$	–	dimensionless coefficients
$s$	–	dimensionless axial transport speed
$t$	–	time
$w$	–	transverse displacement of the beam
$x, y$	–	Cartesian co-ordinates
$z$	–	dimensionless transverse displacement of the beam
$\beta$	–	dimensionless internal damping coefficient
$\varepsilon$	–	strain component in the $x$ direction
$\gamma$	–	internal damping coefficient
$\varepsilon_1, \eta, \kappa$	–	dimensionless coefficients
$\rho$	–	mass density of the beam.

## 1. Introduction

Elastic continua translating at high speed such as band saw blades, magnetic types, paper webs, plastic sheets, films, transmission cables are present in various industrial applications. Excessive vibrations of moving systems increase defects and can lead to failure of the translating materials. The analysis of vibration and dynamic stability of such systems are very important for design of manufacturing devices.

In modeling axially moving materials one can use one-dimensional beam theory (e.g. Wickert, 1992) or two-dimensional plate theory (e.g. Marynowski and Kołakowski, 1999). Although the plate theory gives the most accurate description of physical phenomena that occur in the web, it is very complicated mathematically and requires time-consuming calculations. The previous studies show that for a large class of practically important webs with a small flexural stiffness the beam theory gives equally accurate results as the plate theory (Marynowski, 1999).

The other important problem one can meet while considering axially moving webs is how to model the web material. A lot of earlier works in this field focused on dynamic investigations of string-like and beam-like axially moving isotropic systems (e.g. Wickert and Mote, 1990; Wickert, 1993; Moon and Wickert, 1997). In all these works, the web material was taken to be linearly elastic. However, paper webs, new plastics and composite materials webs, which are used in the industry need more realistic rheologic models. Many investigators studied linear viscoelastic models. Kovalenko (1959) considered

the problem of a column of a constant stiffness with the internal damping linearly proportional to the strain rate. Stevens (1966) considered the stability of an initially straight, simply supported column subjected to an axial load on the assumption that simple spring-dashpot models might adequately represent the column material. Fung et al. (1998) studied transverse vibrations of an axially moving string subjected to an initial stress. The string material was considered as the Kelvin-Voigt element in series with a spring.

In this paper two different rheologic models of the material, namely Kelvin-Voigt and Maxwell ones are used to describe the dynamics of the axially moving beam. Additionally, the results obtained from the analysis of the linearized equations are compared with the results of the integration of the full non-linear equations.

## 2. Mathematical model of the moving beam

A viscoelastic axially moving beam of the length  $l$  is considered. The beam moves with the axial velocity  $c$ . The geometry of the system and the introduced co-ordinates are shown in Fig. 1.

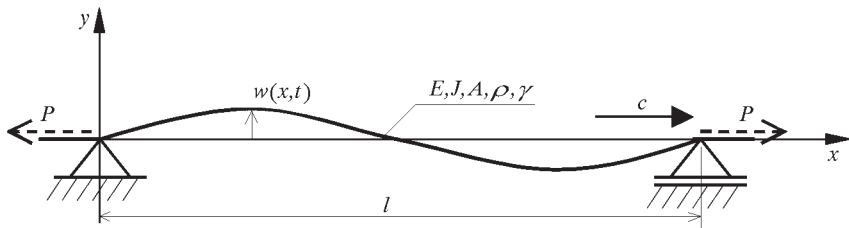


Fig. 1. Axially moving beam

The problem of transverse oscillations of axially moving continua in a state of a uniform initial stress has already been investigated. The results of earlier studies of the axially moving band (Marynowski and Kołakowski, 1999) give the following equation of the beam motion in the  $y$  direction

$$\rho A(-w_{,tt} - 2cw_{,xt} - c^2w_{,xx}) + M_{x,xx} + (N_x w_{,x})_{,x} = 0 \quad (2.1)$$

The uniform initial tension force  $P_0$  provides the required initial stress for the material of the model. The nonlinear strain component in the  $x$  direction is

related to the displacement  $w$  by

$$\varepsilon(x, t) = \frac{1}{2}w_{,x}^2(x, t) \quad (2.2)$$

The one-dimensional constitutive equation of a material of the differential type obeys the relation

$$\Gamma\sigma = \Xi\varepsilon \quad (2.3)$$

where  $\Gamma$  and  $\Xi$  are differential operators defined as

$$\Gamma = \sum_{j=0}^R a_j \frac{d^j}{dt^j} \quad \Xi = \sum_{j=0}^Q b_j \frac{d^j}{dt^j} \quad (2.4)$$

where  $a_j, b_j$  are constant coefficients.

### 2.1. Kelvin-Voigt model of the material

The Kelvin-Voigt rheologic model is shown in Fig. 2a. In this case the differential constitutive equation can be written as

$$a_0\sigma = b_1\varepsilon_{,t} + b_0\varepsilon \quad (2.5)$$

where

$$a_0 = 1 \quad b_0 = E \quad b_1 = \gamma \quad (2.6)$$

To obtain mathematical description of the viscoelastic beam model one should multiply Eq. (2.1) with the operator  $\Gamma$ . The bending moment  $M$  is given

$$M = -EJ_z w_{,xx} - J_z \gamma w_{,xxt} \quad (2.7)$$

Using Eqs (2.2), (2.5) and (2.6) one obtains

$$\begin{aligned} w_{,tt} + 2cw_{,xt} + c^2w_{,xx} + \frac{EJ}{\rho A}w_{,xxxx} + \frac{J\gamma}{\rho A}w_{,xxxxt} - \frac{P_0}{\rho A}w_{,xx} - \frac{3E}{2\rho}w_{,x}^2w_{,xx} - \\ - 2\frac{\gamma}{\rho}(w_{,x}w_{,xt}w_{,xx} + cw_{,x}w_{,xx}^2) - \frac{\gamma}{\rho}(w_{,x}^2w_{,xxt} + cw_{,x}^2w_{,xxx}) = 0 \end{aligned} \quad (2.8)$$

The boundary conditions

$$w(0, t) = w(l, t) = 0 \quad w_{,xx}(0, t) = w_{,xx}(l, t) = 0 \quad (2.9)$$

Let the dimensionless parameters be

$$\begin{aligned}
 z &= \frac{w}{d} & \xi &= \frac{x}{l} & s &= \frac{c}{c_f} = c\sqrt{\frac{A\rho}{P_0}} \\
 \tau &= t\frac{c_f}{l} = \frac{t}{l}\sqrt{\frac{P_0}{A\rho}} & c_f &= \sqrt{\frac{P_0}{A\rho}}
 \end{aligned}
 \tag{2.10}$$

Substitution of Eqs (2.10) into Eq. (2.8) gives a dimensionless nonlinear equation of motion of the Kelvin-Voigt viscoelastic beam

$$\begin{aligned}
 z_{,\tau\tau} + 2sz_{,\xi\tau} + (s^2 - 1)z_{,\xi\xi} + sz_{,\xi} + \varepsilon_1 z_{,\xi\xi\xi\xi} + \beta z_{,\xi\xi\xi\xi\tau} - \frac{3}{2}\kappa z_{,\xi}^2 z_{,\xi\xi} - \\
 - \eta s(2z_{,\xi\xi}^2 z_{,\xi} + z_{,\xi}^2 z_{,\xi\xi\xi}) - \eta(2z_{,\xi} z_{,\xi\tau} z_{,\xi\xi} + z_{,\xi}^2 z_{,\xi\xi\tau}) = 0
 \end{aligned}
 \tag{2.11}$$

where

$$\beta = \frac{J\gamma}{l^3\sqrt{P_0\rho A}} \quad \varepsilon_1 = \frac{EJ}{P_0l^2} \quad \kappa = \frac{Ed^2A}{P_0l^2} \quad \eta = \frac{\gamma d^2A}{l^3\sqrt{P_0\rho A}}
 \tag{2.12}$$

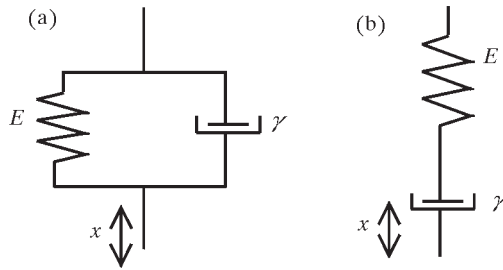


Fig. 2. (a) Kelvin-Voigt and (b) Maxwell rheologic models

### 2.2. Maxwell rheologic model of the material

The Maxwell rheologic model is shown in Fig. 2b. In this case the differential constitutive equation can be written as

$$a_0\sigma + a_1\sigma_{,t} = b_1\varepsilon_{,t}
 \tag{2.13}$$

where

$$a_0 = E \quad a_1 = \gamma \quad b_1 = E\gamma
 \tag{2.14}$$

To obtain mathematical description of the viscoelastic beam model one should multiply Eq. (2.1) with the operator  $\Gamma$  and using Eqs (2.2) and (2.3) one obtains

$$\begin{aligned} & w_{,ttt} + 3cw_{,xtt} + (3c^2 - c_f^2)w_{,xxt} + c(c^2 - c_f^2)w_{,xxx} + r_1w_{,tt} + \\ & + 2r_1cw_{,xt} + r_1(c^2 - c_f^2)w_{,xx} + r_2w_{,xxxx} = \\ & = r_3(2w_{,x}w_{,xt}w_{,xx} + 2cw_{,x}w_{,xx}^2 + w_{,x}^2w_{,xxt} + cw_{,x}^2w_{,xxx}) \end{aligned} \quad (2.15)$$

where

$$c_f = \sqrt{\frac{P_0}{A\rho}} \quad r_1 = \frac{E}{\gamma} \quad r_2 = \frac{E^2 J}{A\rho\gamma} \quad r_3 = \frac{E}{\rho} \quad (2.16)$$

The boundary conditions and the dimensionless parameters are given in Eqs (2.9) and (2.10), respectively. Substitution of Eqs (2.10) into Eq. (2.15) gives a dimensionless nonlinear equation of motion of the Maxwell viscoelastic beam

$$\begin{aligned} & z_{,\tau\tau\tau} + k_1z_{,\tau\tau} + 3sz_{,\xi\tau\tau} + (3s^2 - 1)z_{,\xi\xi\tau} + 2sk_1z_{,\xi\tau} + \\ & + k_1(s^2 - 1)z_{,\xi\xi} + s(s^2 - 1)z_{,\xi\xi\xi} + k_2z_{,\xi\xi\xi\xi} = \\ & = k_3(2z_{,\xi}z_{,\xi\tau}z_{,\xi\xi} + 2sz_{,\xi\xi}^2z_{,\xi} + z_{,\xi}^2z_{,\xi\tau} + sz_{,\xi}^2z_{,\xi\xi\xi}) \end{aligned} \quad (2.17)$$

where

$$k_1 = \frac{El}{\gamma c_f} \quad k_2 = \frac{E^2 J}{P_0 l \gamma c_f} \quad k_3 = \frac{d^3 AE}{P_0 l^2} \quad (2.18)$$

### 2.3. Solution to the problem

The problems represented by Eq. (2.11) for the Kelvin-Voigt rheologic model of the beam material and Eq. (2.17) for the Maxwell one together with the boundary conditions given in Eqs (2.9) have been solved using the Galerkin method. The following finite series representation of the dimensionless transverse displacement has been assumed

$$z(\xi, \tau) = \sum_{i=1}^n \sin(i\pi\xi)q_i(\tau) \quad (2.19)$$

where  $q_i(\tau)$  is the generalized displacement.

Substituting Eq. (2.19) into Eqs (2.11), (2.17) and using the orthogonality condition one determines a set of ordinary differential equations. Sets of the ordinary equations are shown in Appendix for  $n = 3$ .

### 3. Numerical results and discussion

Numerical investigations have been carried out for the beam model of the steel web. Parameters data: length  $l = 1$  m, width  $b = 0.2$  m, thickness  $d = 0.0015$  m, mass density  $\rho = 7800$  kg/m<sup>3</sup>, Young's modulus:  $E = 0.2 \cdot 10^{12}$  N/m<sup>2</sup>, initial stress  $N_0 = 2500$  N/m,  $n = 3$ . Initial conditions:  $q_1 = 1$ ,  $q_{1,t} = 0$ , ...  $q_{3,ttt} = 0$ . The Runge-Kutta method was used to integrate the ordinary differential equations and analyse the dynamic behaviour of the system.

#### 3.1. Kelvin-Voigt model of material

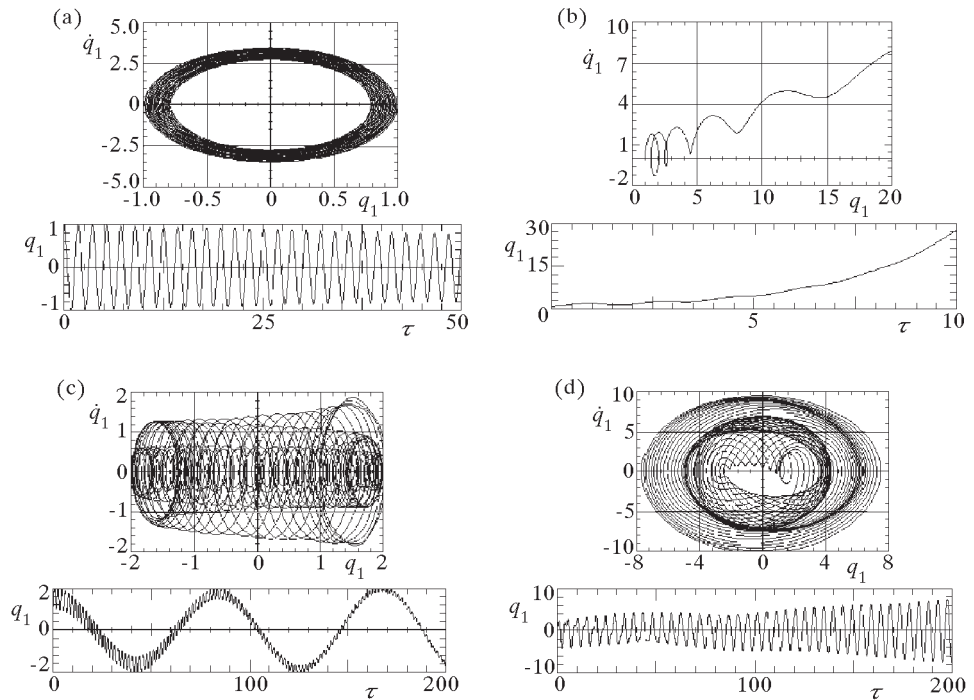


Fig. 3. Phase portrait and time history of the solution of the linearized system (A.1); (a) -  $s = 0$ ,  $\beta = 10^{-4}$ ; (b) -  $s = 1.4$ ,  $\beta = 10^{-4}$ ; (c) -  $s = 1.41$ ,  $\beta = 10^{-5}$ ; (d) -  $s = 1.45$ ,  $\beta = 10^{-5}$

At first, the linearized damped system was investigated. To show the dynamic behaviour of the system natural damped oscillations of the first generalized coordinate  $q_1$  for different values of the axial speed  $s$  of the beam model were

investigated. In the subcritical region of transport speeds ( $s < s_{cr}$ ) one can observe free flexural damped vibrations around the trivial equilibrium position (Fig. 3a). In supercritical transport speeds ( $s > s_{cr}$ ) for a small internal damping the web experiences divergent instability (Fig. 3b) and next flutter instability (Fig. 3d). Between these two instability regions there is a second stability domain. The existence of the second stable region is dependent on the internal damping of the web material. When the internal damping increases the width of the second stable region decreases. The time history of the first generalized coordinate  $q_1$  in the second stable region is shown in Fig. 3c. The location of the instability regions of the linearized system with the Kelvin-Voigt model of an axially moving material is shown in Fig. 4.

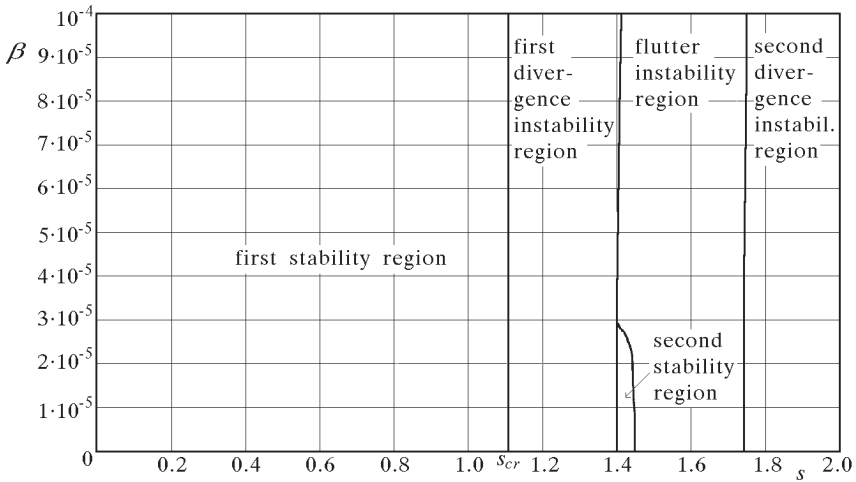


Fig. 4. Instability regions of the linearized system with the Kelvin-Voigt rheologic model of the axially moving material

Subsequently, the non-linear system with the Kelvin-Voigt model of material was investigated. A bifurcation diagram of the non-linear system for the internal damping coefficient  $\beta = 10^{-5}$  is shown in Fig. 5. The dimensionless transport speed  $s$  has been used as the bifurcation parameter. One can observe supercritical bifurcation at the transport speed  $s = s_{cr} = 1.12$ . For  $s < s_{cr}$  only one attractor exists ( $q_1 = 0$ ) and for  $s > s_{cr}$  this critical point becomes repeller and one can observe two attractors (non-zero critical points). The phase portraits and time histories of the solutions of the non-linear system are shown in Fig. 6.

It is worth to note that the analysis of the non-linear system does not indicate the existence of various forms of instability regions of the linearized system.

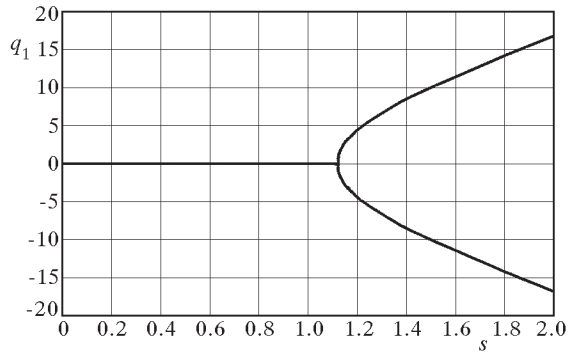


Fig. 5. Bifurcation diagram of the nonlinear system with the Kelvin-Voigt rheologic model of material ( $\beta = 10^{-5}$ )

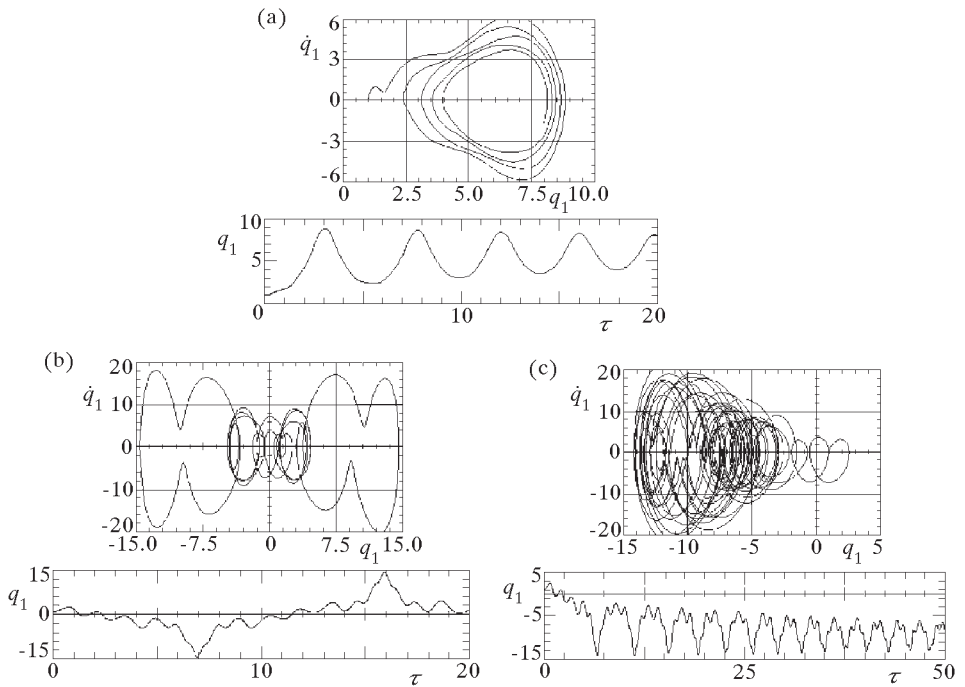


Fig. 6. Phase portrait and time history of the solution of the nonlinear system (A.1);  
 (a) -  $s = 1.3$ ,  $\beta = 10^{-4}$ ; (b) -  $s = 1.54$ ,  $\beta = 0$ ; (c) -  $s = 1.54$ ,  $\beta = 10^{-5}$

Though the analysis of the linearized system predicts exponentially growing oscillations in the divergence instability region of transport speeds, non-linear damped oscillations which tend to the stable critical point occur (Fig. 6a). At transport speeds above the first divergence instability region of the linearized system the undamped non-linear system experiences global motion between two critical points (Fig. 6b). For different values of the internal damping and initial conditions the system may reach various equilibrium positions in the supercritical transport speeds region (Fig. 6c).

### 3.2. Maxwell model of material

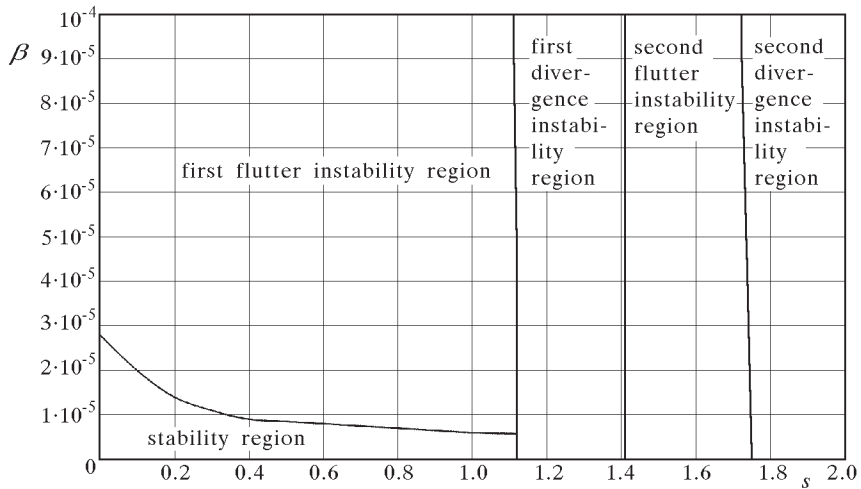


Fig. 7. Instability regions of the linearized system with the Maxwell rheologic model of the axially moving material

The stability and instability regions calculated for the linearized system (A.2) with the Maxwell rheologic model of the beam material are shown in Fig. 7. The results corresponding to the Maxwell model indicate that in the range of supercritical transport speeds only for smaller values of internal damping coefficient ( $\beta < 5 \cdot 10^{-6}$ ) the critical speed of the beam is the same as the one obtained with the Kelvin-Voigt model (compare with Fig. 4). The Maxwell model does not confirm the existence of the second stability region located between the divergence and the flutter instability regions. A phase portrait and time history of oscillations in this region of transport speed are shown in Fig. 8a.

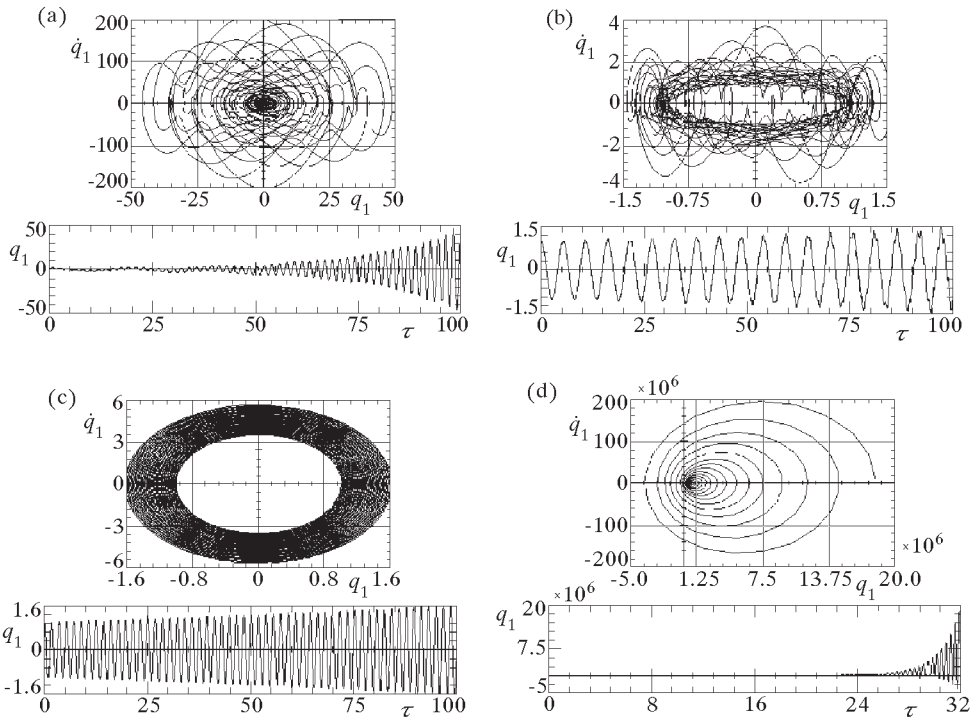


Fig. 8. Phase portrait and time history of the solution of the linearized system (A.2); (a) -  $s = 1.41$ ,  $\beta = 10^{-5}$ ; (b) -  $s = 1.0$ ,  $\beta = 10^{-5}$ ; (c) -  $s = 0$ ,  $\beta = 10^{-4}$ ; (d) -  $s = 1.4$ ,  $\beta = 10^{-4}$

For larger values of the internal damping the system loses its stability due to the flutter instability. This is the significant difference between both considered linearized models, as the Kelvin-Voigt model does not allow the identification of this instability region. The critical value of the transport speed decreases with the increase of the damping coefficient  $\beta$ . The phase portraits and time histories of the system response in both flutter instability regions are shown in Fig. 8b,c,d.

Next, the non-linear system with the Maxwell rheologic model of the axially moving material was investigated. A bifurcation diagram of the non-linear system for the internal damping coefficient  $\beta = 10^{-5}$  is shown in Fig. 9. For  $s < s_{cr} = 0.5$  only one attractor exists ( $q_1 = 0$ ). For  $s > s_{cr}$  one can observe at first the region of transport speeds where unbounded solutions occur. Above this region the non-linear oscillations occur which are characterized by one large limit cycle (region I in Fig. 9). In the second divergence instability region

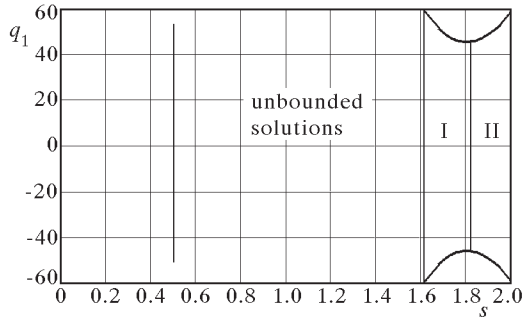


Fig. 9. Bifurcation diagram of the nonlinear system with the Maxwell rheologic model of the axially moving material ( $\beta = 10^{-5}$ , I – large limit cycle region, II – small limit cycle region)

of the linearized system one can observe the non-linear oscillations which are characterized by two small limit cycles (region II in Fig. 9).

The phase portraits and time histories of the system response (the first generalized co-ordinate  $q_1$ ) of the non-linear system for small values of the internal damping co-efficient ( $\beta \leq 10^{-5}$ ) are shown in Fig. 10. At the critical speed the non-linear system exhibits the flatter instability. The characteristic system response in this region is shown in Fig. 10a. Numerical studies of the non-linear system show that in the supercritical range of the transport speed the system exhibits the divergent instability (Fig. 10b). With further increase of the transport speed the large limit cycle oscillations around two equilibria are developed (Fig. 10c). This type of oscillations is similar to the one observed in the Kelvin-Voigt model (Fig. 6b). Phase portraits and time histories of the system response showing the small stable limit cycle around two different equilibria are shown in Fig. 10d,e.

The phase portraits and time histories of the system response (the first generalized co-ordinate  $q_1$ ) of the non-linear system (A.2) for larger values of the internal damping co-efficient ( $\beta > 3 \cdot 10^{-5}$ ) are shown in Fig. 11. Numerical studies of the nonlinear system (A.2) show that in the subcritical range of the transport speed  $s$  one observes damped natural oscillations (Fig. 11a). At the critical transport speed the system loses its stability by divergence. Fig. 11b shows the non-linear system response for  $s \approx s_{cr}$ . The increase of the transport speed and the transition to the divergence instability region of the linearized system (A.2) do not indicate a qualitative change in the response character in comparison with the previous case with small damping.

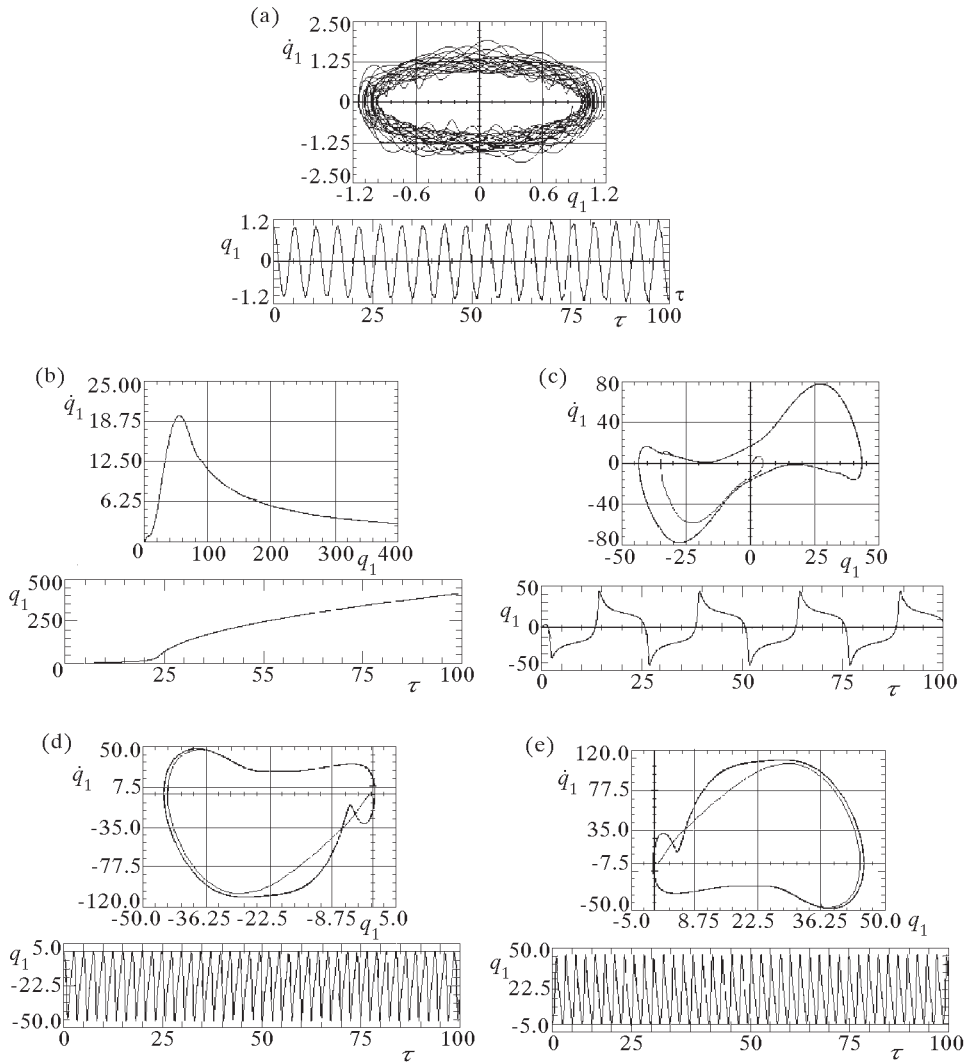


Fig. 10. Phase portrait and time history of the solution of the nonlinear system (A.2); (a) -  $s = 1$ ,  $\beta = 8.9 \cdot 10^{-6}$ ; (b) -  $s = 1.12$ ,  $\beta = 10^{-5}$ ; (c) -  $s = 1.65$ ,  $\beta = 10^{-5}$ ; (d) -  $s = 2$ ,  $\beta = 10^{-5}$ ,  $q_1(0) = -1$ ; (e) -  $s = 2$ ,  $\beta = 10^{-5}$ ,  $q_1(0) = 1$

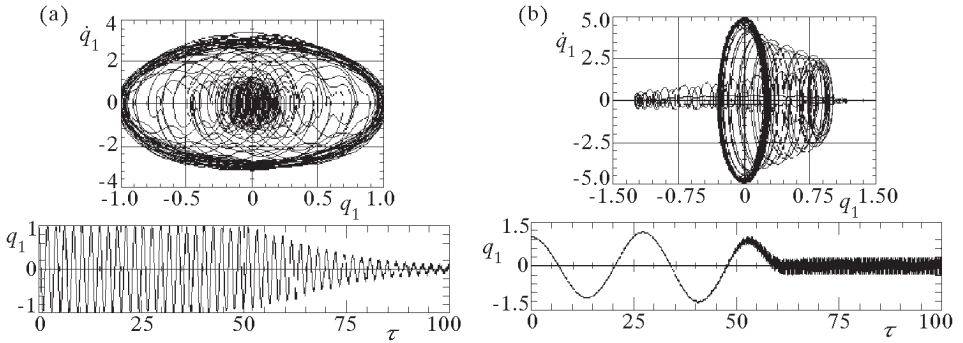


Fig. 11. Phase portrait and time history of the solution of the nonlinear system (A.2); (a) –  $s = 0.5$ ,  $\beta = 3.6 \cdot 10^{-5}$ ; (b) –  $s = 1.11$ ,  $\beta = 3.6 \cdot 10^{-5}$

#### 4. Conclusions

Dynamic investigations of an axially moving beam subject to a constant axial stress are carried out in this paper. As the beam material models the Kelvin-Voigt and Maxwell ones are considered. General forms of differential equations of transverse oscillations of the systems are derived together with the differential constitutive law for their rheologic models.

Numerical investigations have been carried out for the beam model of a steel web. The analysis of the linearized equations with the Kelvin-Voigt material model shows that in the subcritical range of the transport speed an increase in this speed causes a decrease in the frequency of natural oscillations. At the critical speed the system exhibits divergent instability. The analysis of the linearized Maxwell material model shows the system loses its stability due to flutter instability. This is the significant difference between both considered models, as the Kelvin-Voigt model does not allow the identification of this instability region.

For supercritical transport speeds and small internal damping both linearized models show that the system experiences divergent and flutter instabilities. The Kelvin-Voigt model reveals that between these two instability regions there is a second stability area. The width of this region depends on the internal damping of the web material. When the internal damping increases the width of the second stable region decreases more and more and finally disappears. The Maxwell model does not confirm the existence of the second stability region of transport speed.

The dynamic analysis of the non-linear damped system undergoing constant axial stress shows that in the supercritical transport speed region non-trivial equilibrium positions bifurcate from the straight configuration of the web, and global motion between the co-existing equilibrium positions occurs. At the same transport speed, for different values of the internal damping and initial conditions, the system may reach various equilibrium positions. Inside the instability regions one can observe different dynamical behaviour depending on the considered model. The nonlinear Kelvin-Voigt model shows existence of a stable limit cycle in both regions of the divergence instability while the nonlinear Maxwell model indicates such behaviour only in the second region.

The Kelvin-Voigt and Maxwell models give dynamically similar results only for small values of the internal damping ( $\beta < 5 \cdot 10^{-5}$ ). As the experimental estimation of the internal damping in the steel web indicates larger values of  $\beta$  (Osiński, 1997), the description of the dynamical behaviour of such a system requires experimental verification of both considered models.

#### *Acknowledgement*

This paper was supported by the State Committee for Scientific Research (KBN) under grant No. 7 T08E03417.

## A. Appendix

The set of ordinary differential equations of the viscoelastic beam model with the Kelvin-Voigt model of the material ( $n = 3$ )

$$\begin{aligned} \ddot{q}_1 &= (s^2 - 1)\pi^2 q_1 - \varepsilon_1 \pi^4 q_1 + \frac{16}{3} s \dot{q}_2 - \beta \pi^4 \dot{q}_1 - \\ &- a_1 \left( \frac{3}{8} q_1^3 + 3q_1 q_2^2 + \frac{27}{4} q_1 q_3^2 + \frac{9}{8} q_1^2 q_3 + \frac{9}{2} q_2^2 q_3 \right) + \\ &+ a_2 s \left( \frac{848}{21} q_1 q_2 q_3 + \frac{2992}{35} q_2 q_3^2 + \frac{112}{15} q_1^2 q_2 + \frac{1408}{105} q_2^3 \right) - \\ &- a_2 \left( \frac{3}{4} q_1^2 \dot{q}_1 + \frac{3}{4} q_1^2 \dot{q}_3 + \frac{3}{2} q_1 \dot{q}_1 q_3 + 3q_2^2 \dot{q}_3 + \right. \\ &+ \left. 6q_2 \dot{q}_2 q_3 + 4q_1 q_2 \dot{q}_2 + 2\dot{q}_1 q_2^2 + \frac{9}{2} \dot{q}_1 q_3^2 + 9q_1 q_3 \dot{q}_3 \right) \\ \ddot{q}_2 &= 4(s^2 - 1)\pi^2 q_2 - 16\varepsilon_1 \pi^4 q_2 - \frac{16}{3} s \dot{q}_1 + \frac{48}{5} s \dot{q}_3 - 16\beta \pi^4 \dot{q}_2 - \end{aligned}$$

$$\begin{aligned}
& - a_1(3q_1^2q_2 + 6q_2^3 + 27q_2q_3^2 + 9q_1q_2q_3) + \\
& + a_2s\left(\frac{8}{15}q_1^3 + \frac{44712}{385}q_3^3 + \frac{1952}{105}q_1q_2^2 + \frac{1016}{35}q_1q_3^2 + \frac{936}{35}q_1^2q_3 + \frac{1568}{15}q_2^2q_3\right) - \\
& - a_2(6q_1q_2\dot{q}_3 + 6q_1\dot{q}_2q_3 + 12q_2^2\dot{q}_2 + 6\dot{q}_1q_2q_3 + \\
& + 4q_1\dot{q}_1q_2 + 36q_2q_3\dot{q}_3 - \frac{27}{2}q_1q_3\dot{q}_3 + 2q_1^2\dot{q}_2 + 18q_3^2\dot{q}_2) \\
\ddot{q}_3 = & 9(s^2 - 1)\pi^2q_3 - 81\varepsilon_z\pi^4q_3 - \frac{48}{5}s\dot{q}_2 - 81\beta\pi^4\dot{q}_3 - \\
& - a_1\left(\frac{3}{8}q_1^3 + \frac{243}{8}q_3^3 + \frac{9}{2}q_1q_2^2 + \frac{27}{4}q_1^2q_3 + 27q_2^2q_3\right) + \\
& + a_2s\left(-\frac{10656}{105}q_1q_2q_3 + \frac{78192}{385}q_2q_3^2 + \frac{144}{35}q_1^2q_2 - \frac{128}{15}q_2^3\right) - \\
& - a_2\left(\frac{3}{4}q_1^2\dot{q}_1 + \frac{9}{2}q_1^2\dot{q}_3 + 4q_1\dot{q}_1q_2 + \frac{243}{4}q_3^2\dot{q}_3 + \right. \\
& \left. + 9q_1\dot{q}_1q_3 + 2q_1q_2\dot{q}_2 + 3\dot{q}_1q_2^2 + 18q_2^2\dot{q}_3 + 36q_2\dot{q}_2q_3\right)
\end{aligned} \tag{A.1}$$

where

$$\beta = \frac{J\gamma}{l\sqrt{P_0\rho A}} \quad \varepsilon_1 = \frac{EJ}{P_0l^2} \quad a_1 = \frac{Ed^2A\pi^4}{P_0l^2} \quad a_2 = \frac{\gamma d^2A_z\pi^4}{l^3\sqrt{P_0\rho A}}$$

The set of ordinary differential equations of the viscoelastic beam model with the Maxwell model of the material ( $n = 3$ )

$$\begin{aligned}
\ddot{q}_1 = & -k_1\ddot{q}_1 + 8s\ddot{q}_2 - \pi^2(1 - 3s^2)\dot{q}_1 + \frac{16}{3}k_1s\dot{q}_2 - \pi^2[k_1(1 - s^2) + \pi^2k_2]q_1 + \\
& + \frac{32}{3}\pi^2s(1 - s^2)q_2 - 2k_3\pi^4\left(\frac{3}{8}q_1^2\dot{q}_1 + \frac{3}{4}q_1q_3\dot{q}_1 + 3q_2q_3\dot{q}_2 + \right. \\
& + \frac{3}{8}q_1^2\dot{q}_3 + \frac{3}{2}q_2^2\dot{q}_3 + 2q_1q_2\dot{q}_2 + \frac{9}{2}q_1q_3\dot{q}_3 + q_2^2\dot{q}_1 + \frac{9}{4}q_3^2\dot{q}_1) + \\
& + 2k_3s\pi^5(2.134q_2^3 + 1.189q_1^2q_2 + 6.543q_1q_2q_3 + 40.745q_2q_3^2) \\
\ddot{q}_2 = & -k_1\ddot{q}_2 - 8s\ddot{q}_1 - 4\pi^2(1 - 3s^2)\dot{q}_2 - \frac{16}{3}k_1s\dot{q}_1 - 4\pi^2[k_1(1 - s^2) + \\
& + 4\pi^2k_2]q_2 + \frac{72}{5}s\ddot{q}_3 + \frac{48}{5}k_1s\dot{q}_3 - \frac{8}{3}\pi^2s(1 - s^2)q_1 + \frac{216}{5}\pi^2s(1 - s^2)q_3 -
\end{aligned}$$



8. WICKERT J.A., 1992, Nonlinear vibration of a traveling tensioned beam, *Int. Journal of Non-Linear Mechanics*, **27**, 3, 503-517
9. WICKERT J.A., 1993, Analysis of self-excited longitudinal vibration of a moving tape, *Journal of Sound and Vibration*, **160**, 3, 455-463
10. WICKERT J.A., MOTE C.D. JR, 1990, Classical vibration analysis of axially-moving continua, *Journal of Applied Mechanics ASME*, **57**, 738-744

## Nieliniowa analiza dynamiki przesuwającej się osiowo wiskoelastycznej belki

### Streszczenie

W pracy badano stateczność dynamiczną ruchu oraz drgania przesuwającej się osiowo belki. Do opisu własności materiału belki zastosowano dwa modele reologiczne: model Kelvina-Voigta oraz model Maxwella. Dla obu badanych modeli wyprobowano nieliniowe równania różniczkowe o pochodnych cząstkowych opisujące ruch poprzeczny belki. Przybliżone rozwiązanie równań ruchu otrzymano stosując metodę Galerkiną. Badania numeryczne przeprowadzono dla modelu belkowego przesuwającej się osiowo cienkiej wstęgi stalowej. Badano wpływ prędkości przesuwu oraz tłumienia wewnętrznego na stateczność dynamiczną układu. Wyniki badań wskazują, że tylko przy małych wartościach bezwymiarowego współczynnika tłumienia wewnętrznego  $\beta < 5 \cdot 10^{-6}$  układy z obydwoma badanymi modelami reologicznymi charakteryzują się podobnym zachowaniem dynamicznym. Przy wyższym tłumieniu wewnętrznym otrzymano różniące się wyniki badań dynamiki zarówno układu zlinearyzowanego, jak i układu nieliniowego.

*Manuscript received May 28, 2001; accepted for print October 1, 2001*